Molecular BioSystems

Cite this: *Mol. BioSyst.*, 2011, **7**, 1241–1253

www.rsc.org/molecularbiosystems

PAPER

A metabolomics and proteomics study of the adaptation of *Staphylococcus aureus* to glucose starvation†

Manuel Liebeke,‡[a] Kirsten Dörries,‡[a] Daniela Zühlke,‡[b] Jörg Bernhardt,[b] Stephan Fuchs,[b] Jan Pané-Farré,[b] Susanne Engelmann,[b] Uwe Völker,[c] Rüdiger Bode,[b] Thomas Dandekar,[d] Ulrike Lindequist,[a] Michael Hecker[b] and Michael Lalk*[a]

Received 6th December 2010, Accepted 25th January 2011
DOI: 10.1039/c0mb00315h

As a versatile pathogen *Staphylococcus aureus* can cause various disease patterns, which are influenced by strain specific virulence factor repertoires but also by *S. aureus* physiological adaptation capacity. Here, we present metabolomic descriptions of *S. aureus* central metabolic pathways and demonstrate the potential for combined metabolomics- and proteomics-based approaches for the basic research of this important pathogen. This study provides a time-resolved picture of more than 500 proteins and 94 metabolites during the transition from exponential growth to glucose starvation. Under glucose excess, cells exhibited higher levels of proteins involved in glycolysis and protein-synthesis, whereas entry into the stationary phase triggered an increase of enzymes of TCC and gluconeogenesis. These alterations in levels of metabolic enzymes were paralleled by more pronounced changes in the concentrations of associated metabolites, in particular, intermediates of the glycolysis and several amino acids.

Introduction

Staphylococcus aureus is a versatile pathogen responsible for a wide range of nosocomial infections in humans and animals. As a commensal microorganism *S. aureus* is found on mucosa and skin. More severe forms of staphylococcal infections are endocarditis, osteomyelitis, sepsis and the toxic shock syndrome.[1] *S. aureus* is able to express a large number of virulence factors like cell-surface exposed proteins, enzymes and toxins supporting invasion of tissues and cells. Survival within the host is accomplished by integration of adaptive responses at the gene expression and the metabolic level as well as exploiting defined structural and functional features of virulence factors.[2] This interplay between eukaryotic host and bacterial pathogens shapes the virulence factor expression profile and metabolism. Pathogenic bacteria have important metabolite-sensing regulators like the carbon catabolite protein A (CcpA) and CodY which control both metabolic as well as virulence genes, therefore connecting metabolism with virulence.[3–6] Precise fine-tuning of the activity of tricarboxylic acid cycle (TCC) enzymes is also critical for virulence of *S. aureus*.[7] Artificially high activity of the TCC in a *glnP* mutant caused reduced production of polysaccharide intercellular adhesin (PIA) and reduced *in vivo* virulence of *S. aureus* in an endocarditis model of device-associated biofilms and in kidney and spleen.[7] Inactivation of TCC on the other hand triggered reduction of capsule synthesis.[8] The interplay between metabolism of staphylococci and their virulence factor synthesis has been recently reviewed[9] and shows the remarkable impact of metabolism on virulence.

Due to their ability to capture changes at a genome wide scale functional genomics approaches can provide new insights into these complex networks and reveal new facets of the interplay between gene regulation, protein synthesis, metabolism and pathogenicity. For *S. aureus*, genome sequences have been determined for a number of laboratory strains as well as clinically important isolates.[10–12] These sequences provide the framework for extensive transcriptional and proteomic analysis of the *S. aureus* response to a number of infection mimicking cues.[13] This information has been exploited for metabolic network reconstructions,[14,15] but detailed metabolite data are still missing. Such metabolome data would provide the ability to assess the degree by which the modifications of the gene expression and protein network

[a] *Institute of Pharmacy, Ernst-Moritz-Arndt-University Greifswald, F.-L.-Jahn-Str. 17, D-17487 Greifswald, Germany. E-mail: lalk@uni-greifswald.de; Fax: +49 3834-864885; Tel: +49 3834-864867*
[b] *Institute for Microbiology, Ernst-Moritz-Arndt-University Greifswald, F.-L.-Jahn-Str. 15, D-17487 Greifswald, Germany*
[c] *Interfaculty Institute for Genetics and Functional Genomics, Ernst-Moritz-Arndt-University Greifswald, F.-L.-Jahn-Str. 15a, D-17487 Greifswald, Germany*
[d] *Bioinformatik, Biozentrum, Am Hubland, University of Wuerzburg, D-97074, Germany*
† Electronic supplementary information (ESI) available. See DOI: 10.1039/c0mb00315h
‡ These authors contributed equally to this work.

translate into changes in metabolic activity and thus allow an integrated, systems biology-like analysis of bacterial physiology. The value of such data has been nicely demonstrated for *Escherichia coli*[16,17] and *Pseudomonas putida*.[18] For *S. aureus*, *in silico* predictions assumed approximately 700 metabolic processes connecting 571–712 metabolites in the metabolic network,[15,19] whereas other groups calculated approx. 1200 reactions connecting about 1400 metabolites.[20] Analysis of the central carbon core metabolism revealed that *S. aureus* is able to utilize glucose *via* glycolysis (Embden–Meyerhoff pathway, EMP), the pentose-phosphate pathway (PPP) and the TCC. In natural settings *S. aureus* frequently encounters limiting nutrient supply and thus its metabolic activities are precisely adjusted to ensure competitiveness and survival. Almost all of the metabolic enzymes of *S. aureus* are amenable to proteomic analysis[13] and extensive changes in the cytosolic subproteome have been recorded during the transition of *S. aureus* from the exponential to the stationary phase in a nutrient rich complex medium.[13,21] Proteins involved in transcription, protein synthesis and glycolysis were strongly expressed in the exponential growth phase. In contrast, in the stationary phase the enzyme levels of the TCC and gluconeogenesis pathways were increased.[13,21]

In the current study, we further investigate the adaptation of *S. aureus* to this physiologically relevant nutrient limitation and provide for the first time an integrated view of time resolved changes in the metabolome and proteome of *S. aureus* during adaptation to glucose starvation.

Material and methods

Bacterial strain, media and culture conditions

Wild type *S. aureus* COL[22] was cultivated in a chemically defined medium (CDM)[23] with 7.5 mM glucose, 0.142 mM citrate, 1 mM amino acids each (alanine, threonine, serine, leucine, isoleucine, valine, proline, glutamic acid, aspartic acid, arginine, phenylalanine, tryptophan, histidine, cysteine, lysine) and specific vitamins and trace elements, but without 3-(*N*-morpholino)propanesulfonic acid buffer. Growth conditions were as previously reported,[24] overnight cultures in CDM were diluted to an optical density at 500 nm (OD_{500}) of 0.07 in 1 L fresh CDM in a 5 L baffled shake flask. At OD_{500} 0.5 the culture was split into eight 60 mL aliquots, transferred into 500 mL shaking flasks and cultivated until sampling. Sampling for metabolome and proteome measurements was done at OD_{500} 0.5 (time point t_0: 0 hour) and 1, 3, 5, 7, 9, 13, 19, 24 hours (time points t_x: x = 1, 3, 5, 7, 9, 13, 19, 24) later.

Processing of samples for metabolome analyses

For intracellular metabolite analysis cells were harvested according to the previously described fast filtration approach.[25] Briefly, cells from suspensions were filtered with a 0.45 μm pore size filter on a vacuum filter system. Cells were washed twice with ice-cold NaCl-solution of the same osmolarity as the medium. Filters with cells were immediately quenched in cold extraction solution (60% w/v. ethanol/water) and subsequently frozen in liquid nitrogen. Cell disruption and metabolite extraction were done with glass beads according to Meyer *et al.*[25] Extracts were lyophilized to complete dryness. For analysis of extracellular metabolites 2 mL of cell suspension were sterile filtered on ice by using a 0.45 μm pore size filter to obtain cell-free extracellular metabolite samples as described recently.[26] All filtrates were stored at −20 °C until measurement.

Metabolome analysis

Extracted intracellular metabolites were analyzed by liquid chromatography–mass spectrometry (LC-MS) after redissolving the dried extract in 100 μL of ultra pure water. Chromatography conditions and parameters of the mass spectrometer are described elsewhere.[27,28] Mass spectral tags were extracted and integrated using Bruker DataAnalysis Vers. 3.4 (Bruker Biospin) and QuantAnalysis Vers. 1.8 (Bruker Biospin). All peak areas were normalized to Br-ATP, which served as the internal standard in all samples.

Additionally, all extracts of intracellular metabolites were analyzed by gas chromatography–mass spectrometry (GC-MS). For this reason, a sample identical to that used for LC-MS was derivatized with MeOx (methoxyamine) and MSTFA (*N*-methyl-*N*-trimethylsilyltrifluoroacetamide) and injected into GC-MS. Details of derivatization and GC-MS conditions were described recently.[29] Data analysis was performed with the exported netCDF files (Chemstation Vers. E.02.00 Service Pack 2, Agilent) by Metaquant Ver. 1.3.[30] Peak areas of extracted ions were normalized to the internal standard ribitol.

For extracellular metabolome analysis ^{1}H-NMR analysis was done in 5 mm glass tubes (7 inch in length; NORELL ST-500) in which 400 μL of sample were buffered to pH 7.0 by adding 200 μL 0.2 M sodium hydrogen phosphate buffer solution made up with 50% D_2O which provides a nuclear magnetic resonance (NMR)-lock signal. Additionally the buffer solution contains 1 mM TSP (3-trimethylsilyl-[2,2,3,3-D_4]-1-propionic acid) as an internal standard for subsequent quantification. ^{1}H-NMR analysis and quantitative evaluation was carried out as described previously.[26]

Calculation of intracellular metabolite concentrations

Ratios of peak areas to the respective internal standard were used for absolute quantification. Calibration curves of pure substances were measured over a wide range of concentrations under the same conditions and were used for the calculation of metabolite concentration. Quantification was done relative to the internal standard, if no calibration was performed with pure compounds. Metabolite concentrations were reported on a cell dry weight (CDW) basis.[25]

Statistics and visualization of metabolome data

The metabolite results were imported into an Excel® (Microsoft®) sheet which served as an input file for Vanted Vers. 1.66 software, generating time resolved plots of metabolite concentrations.[31] Heat maps were created with TIGR Multi-Experiment-Viewer Vers. 4.2 from TAB delimited text files of metabolite data,[32] by displaying ratios

of determined metabolite levels (mean value of 3 replicates) and the corresponding control values described in each figure legend. Hierarchical clustering (HCL) of metabolite profiles (mean values from three independent experiments) was also performed with TMEV by using the following parameters: complete linkage, Euclidean distance, leaf order optimization. For the calculation of statistically significant alterations two tailed Student's *t*-test was performed in Excel® (Microsoft®).

Processing of samples for proteome analysis

For isolation of intracellular proteins 50 mL of bacterial culture were harvested. After centrifugation (10 min, 4 °C, 8000 rpm) cell pellets were washed with and resuspended in 1 mL TE buffer (10 mM Tris, 1 mM EDTA, pH 7.5). Cells were added to 500 µL of glass beads with 0.1 mm diameter and disrupted using the Precellys 24 homogenizer (Peq Lab, Germany) for 30 s at 6800 rpm. Cell debris and glass beads were separated from the proteins by centrifugation for 10 min at 4 °C at 15 000 rpm followed by a second centrifugation step to remove insoluble and aggregated proteins (30 min, 4 °C, 15 000 rpm).

Protein concentrations of crude extracts were determined using a Ninhydrin assay.[33] 2D electrophoresis was carried out as described earlier.[34] In the first dimension, 70 µg of the total protein extract were loaded onto IPG strips covering the pI range of 4–7 (GE Healthcare). After separation of the proteins in the second dimension 2D gels were fixed with 40% ethanol and 10% acetic acid, subsequently stained with fluorescent Krypton dye according to the manufacturer's instructions (Thermo Scientific) and scanned with a Typhoon 9400 scanner (Amersham Biosciences; excitation source: 532 nm laser, emission filter: 560 nm longpass, resolution 200 µm). Image analysis and spot quantitation was done with the Delta2D software 4.0 (Decodon GmbH, Germany). Gels were warped, spots were detected on a fusion gel image generated with the default parameters and subsequently the resulting spot consensus was transferred back to the original gel images to ensure uniform spot detection and quantification across all gels.[35] Identification of protein spots was done with the help of a recently created reference map of cytosolic proteins of *S. aureus* COL.[13] Labels from this reference map were transferred manually to the fusion gels. Individual spot volumes were normalized to the sum of volumes of all spots detected on the gel to correct for variations in gel loading. For comparisons of protein amounts between different time points a minimal change of 2.0 was defined as relevant. For additional statistical analysis selected proteome data were loaded in TMEV 4.5.1.[32] Significantly changed expression profiles were detected by using one-way ANOVA ($\alpha = 0.05$, distribution based on 1000 permutations). Furthermore, hierarchical sample clustering (HCL) shown in this study was done using complete linkages and Euclidean distances. In addition, calculations of metabolite/protein correlations were performed with the above mentioned software. Therefore fold-changes of proteins and metabolites (value t_x/t_0) were used in a single data matrix to perform HCL (complete linkages, Pearson correlation) and gene distance matrix visualization based on Pearson correlation.

Results and discussion

General overview of metabolome and proteome analysis

The combination of proteome and metabolome approaches is particularly useful if time-resolved data sets are generated because changes in the amount of proteins and metabolites can then be correlated (see Fig. 1) providing new insights into regulation of *S. aureus* metabolism. In total we quantified 94 intracellular metabolites and 531 proteins in a time dependent fashion. Representative metabolome (GC-MS chromatogram overlay) and proteome data (2D-gel overlay) with obvious changes between growing (glucose excess) and non-growing (glucose starvation) cells are presented in Fig. S1, ESI.† A hierarchical cluster analysis resulted in five main clusters for metabolite and protein level alterations during the experiment (see Fig. 1) and shows that a majority of metabolite and proteins of central pathways decreased during glucose starvation, but a certain amount of accumulations were also observed. A distance matrix calculation visualized the overall correlation between metabolites/proteins and between both metabolite/metabolite as well as protein/protein and gives first implications for similar or converse behaving molecules.

Changes of extracellular metabolites in the chemically defined medium during growth of *S. aureus* COL

S. aureus COL was grown in CDM under vigorous agitation at 37 °C. After 9 hours, cultivated cells reached the stationary phase at an $OD_{500} = 2.5$ (see Fig. 2A). At selected time points (starting at $OD_{500} = 0.5$) samples were taken in exponential, transient and stationary growth phases for proteome and metabolome analysis. For analysis of consumption and secretion of extracellular metabolites, a detailed quantification of all compounds in CDM before inoculation and at defined time points during growth was carried out by ^{1}H-NMR spectroscopy. Changes of metabolite concentrations are displayed in Fig. 2B as a color coded heat map. Glucose as the main carbon source was the most consumed of all medium compounds and was completely exhausted at t_9, when *S. aureus* COL entered the stationary phase (Fig. 2A). In order to prove that *S. aureus* was indeed starved for glucose, in a parallel experiment glucose was re-added in the stationary phase, which instantly reestablished growth (Fig. S2, ESI†). The selected timescale allowed a monitoring of alterations in the metabolome during growth (t_0–t_3), for the transition to the stationary phase (time points t_5–t_9) as well as during extended starvation for glucose (t_{13}–t_{24}). Acetate, a known overflow metabolite of aerobically growing *S. aureus*, was the most abundantly secreted metabolite in the cell supernatant, which was secreted as long as glucose was detected in the supernatant and then was consumed again after glucose had been exhausted (Fig. 2A). In fact, consumption of previously secreted acetate by glucose starved *S. aureus* COL has been described before.[36,37] However, not all *S. aureus* strains are able to reuse secreted acetate.[38] Amongst others, pyruvate, lactate, 2,3-butandiol, 2-oxoglutarate, succinate and fumarate were detected as secretion products. These metabolites were secreted during exponential and transient growth phases and subsequently consumed in the stationary phase. In addition,

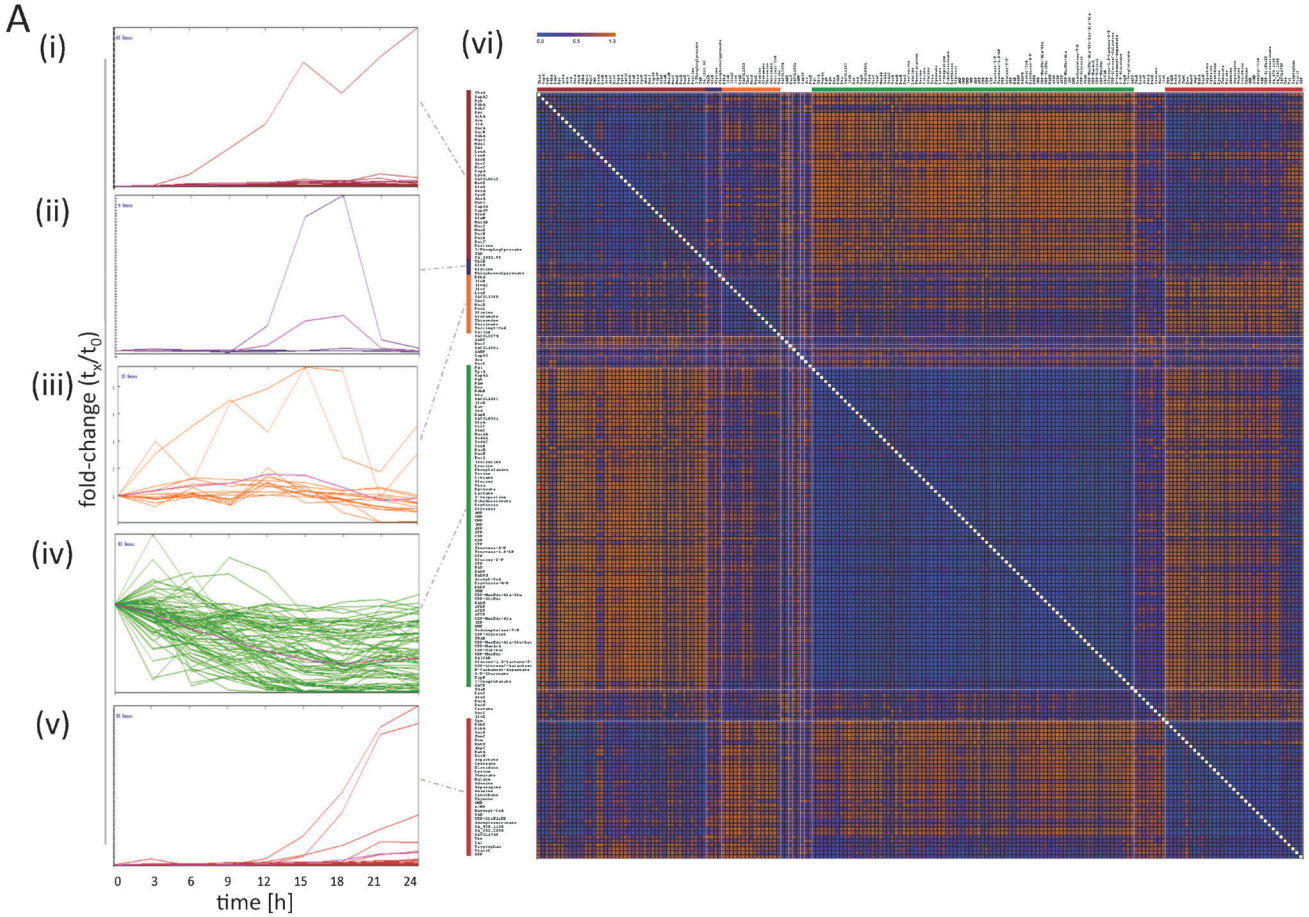

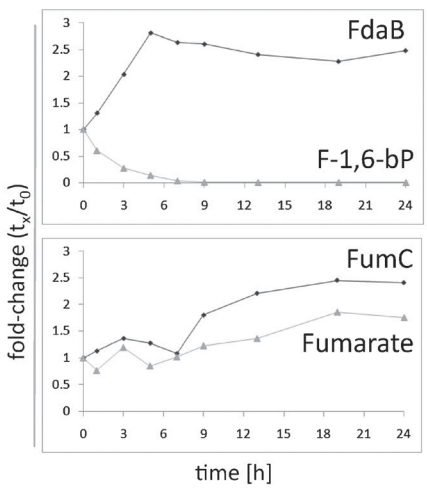

C

pathway	protein/metabolite	corr.
glycolysis, gluconeogenesis, PPP, pyruvate metabolism	FdaB / fructose-1,6-bP	- 0.920
	Zwf / Glucono-1,5-lactone-6-P	- 0.912
TCC	Acn / citrate	- 0.955
	FumC / fumarate	+ 0.915
cell wall metabolism	GlmS / fructose-6-P	- 0.965

Fig. 1 Clustering and correlations between metabolite and protein data. (A) Main clusters of a hierarchical clustering analysis are shown in (i–v), representing >90% of all analyzed proteins of the central carbon metabolism and metabolites. Cluster (i) (dark red) includes 43 variables increasing during the experiment, cluster (ii) (purple) includes 4 variables having a maximum between t_9 and t_{13}, cluster (iii) (orange) includes 25 variables showing an initial increase and afterwards decrease, cluster (iv) (green) represents 82 variables showing decreased levels during the experiment, cluster (v) (light red) displays 35 variables with an increase in stationary phase. In (vi) a distance matrix for all analyzed metabolites and central pathway proteins was used to display distances between two variables, inverse of similarity, as calculated using a distance metric. The distance matrix gives an intuitive and comprehensive view of distance (or similarity) between any two variables by creating a colored matrix representing all variable-to-variable distances based on Pearson correlation. High similarity between two variables is shown by blue colored boxes as demonstrated in the example (B) between fumarate hydratase (FumC) and fumarate. A high inverse similarity between variables is shown by orange colored boxes and is displayed in (B) for fructose-bisphosphate aldolase (FdaB) and fructose-1,6-bisphosphate levels. Examples for high similar or inverse similar protein–metabolite pairs in central pathways are given in (C), all calculated distances are available in Table S1, ESI.† For all calculations fold-ratios ($value_{tx}/value_{t0}$) were used.

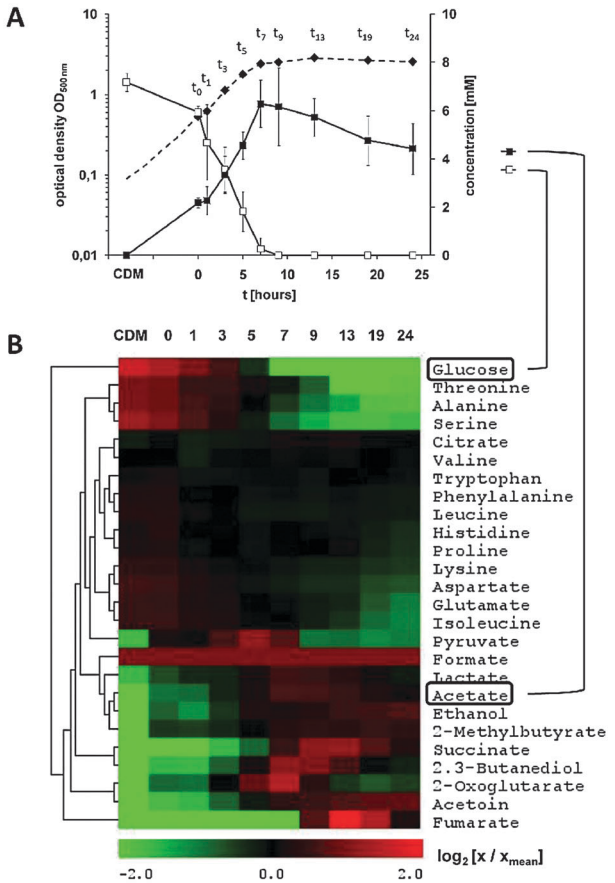

Fig. 2 (A) *S. aureus* COL growth curve in CDM (dashed line) with sample time points marked (filled diamonds). Sampling was started at OD_{500} of 0.5 with time point 0 h. Glucose (open squares) and acetate (filled squares) concentrations are shown in mM. (B) Time-resolved extracellular metabolite values were visualized with TMEV as color coded chart $\log_2 (x/x_{mean})$. Green colorations display lower than average concentrations whereas red colorations represent higher than average concentrations of extracellular metabolites. Red colorations in late stationary phase are correlated with secretion of metabolites. Metabolites are ordered by hierarchical cluster analysis.

acetoin, ethanol and 2-methylbutyrate were secreted in small amounts and the levels steadily increased during the experiment. The levels of citrate, which could constitute an additional carbon source, did not significantly change during growth and glucose starvation of *S. aureus* COL. For the 15 amino acids that were present in CDM different uptake patterns emerged. While threonine, alanine and serine were rapidly consumed, lysine, aspartate, glutamate and isoleucine levels decreased slowly, but there was no remarkable consumption of aromatic amino acids (see Fig. 2B and Table S2a, ESI†).

Time resolved analysis of intracellular metabolites—a global perspective

A defined list of 94 mass spectral tags was evaluated across all samples in both GC-MS and LC-MS chromatograms (see Table 1 and Table S2b, ESI†). Overall we identified 78 metabolites by pure chemical standard comparisons,[39] determined absolute concentrations of 56 metabolites and monitored changes in the absolute and relative concentrations in *S. aureus* during the transition from growth to glucose starvation (Fig. 3).

In *S. aureus* absolute concentrations of metabolites differed by up to $>10^4$ fold. For example GMP was detected at a cellular concentration of 0.01 μmol g^{-1} CDW whilst glutamate, the most abundant metabolite in exponentially growing cells, was measured at 500 μmol g^{-1} CDW (see Table 1). Comparison of *S. aureus* cells growing with an excess of glucose (exponential growth, $OD_{500} = 0.5$) with those extensively starved of glucose demonstrated significant alterations in the intracellular metabolite pool (see Fig. 3). The ratio-plot, which is displayed in Fig. 3, illustrates the strong stationary-phase associated reductions in levels of glycolysis intermediates, nucleotides, selected amino acids such as serine and leucine and intermediates of cell wall metabolism. *Vice versa*, increased levels in the stationary phase were mainly detected for amino acids like ornithine, lysine and histidine. Overall the numbers of metabolites which increased or remained constant or decreased during the experiment showed normal distribution between those classes (see Fig. 4A). In order to better define the influence of glucose starvation on the different branches of metabolism the time resolved patterns of metabolite levels were subjected to hierarchical clustering (HCL) (see Fig. 4A). As expected metabolites of central carbon metabolism and selected intermediates connected to energy metabolism were arranged in the same cluster and displayed a consistent decrease in concentration in the stationary phase (see Cluster 1, Fig. 4A). A second cluster (Cluster 2, Fig. 4A) displayed a less pronounced and often transient decrease or increase in concentrations of intracellular metabolites. This cluster was comprised of various amino acids (thr, ser, leu, phe, trp, pro, ile, glu, val and ala) as well as compounds involved in purine and pyrimidine metabolism. For some amino acids (his, asp, asn, cys, orn, lys and gly) an increase in concentration was detected only during glucose starvation (see, Cluster 3, Fig. 4A).

A proteomic view of the adaptation of *S. aureus* to glucose starvation

In the analytical window of the 2D gel covering a pI range from 4–7 and a mass range of 10–140 kDa two-thirds (~1200 proteins) of the cytosolic proteins of *S. aureus* can theoretically be detected.[21] Our proteome analysis covered about 900 spots of which 637 spots were identified by mass spectrometry on a reference map.[13] Since proteins may be represented by multiple spots due to modifications changing either the molecular weight and/or the isoelectric point, the 637 spots were assigned to 531 different proteins. Comparative quantitative analysis of the protein patterns to that of exponentially growing cells ($OD_{500} = 0.5$) revealed three different classes of proteins: (i) proteins, whose level strongly increased during entry into the stationary phase, (ii) proteins, the level of which did not respond to the nutrient status and (iii) proteins which were present at diminished levels in the stationary phase compared to exponentially growing cells (see Fig. S1 and S3, ESI†). Applying a cut-off value of a minimum fold change in intensity of 2-fold we found 48 spots with significantly increasing intensity and 9 protein spots whose intensity clearly decreased in response to glucose

Table 1 Intracellular metabolite concentrations for nine sample time points (see Fig. 2 for growth curve), absolutely quantified and normalized to CDW [μmol g^{-1} CDW]. Metabolites were determined with GC-MS and LC-MS measurements. Data represent mean values of 3 biological replicates. CDW = cell dry weight. The corresponding standard deviations are listed in Table S2c, ESI†

	Time [h]								
Metabolite	0	1	3	5	7	9	13	19	24
Adenine	0.30	0.22	0.20	0.17	0.27	0.32	0.40	0.58	0.53
ADP	4.47	3.87	2.23	1.68	2.70	2.45	1.32	2.11	2.68
Alanine	302.68	268.33	326.79	262.68	436.06	309.16	209.13	148.78	121.12
AMP	1.56	1.71	0.36	0.52	0.65	0.77	0.33	0.91	0.91
Asparagine	0.20	0.19	0.21	0.17	0.26	0.33	0.37	0.64	0.53
Aspartate	149.75	110.20	120.24	84.26	302.02	324.87	318.02	562.14	593.47
ATP	14.35	12.77	13.29	9.45	9.04	6.66	4.77	4.44	4.44
CDP	1.04	0.94	0.62	0.58	0.54	0.47	0.37	0.84	0.83
Citrate	5.10	5.13	5.79	4.56	3.56	2.15	1.50	1.71	2.34
CMP	1.37	1.02	0.51	0.30	0.32	0.12	0.21	0.70	0.61
CTP	2.79	2.51	2.52	1.69	1.62	0.96	0.94	1.59	1.74
Cysteine	0.88	2.00	1.74	2.23	2.02	1.52	2.00	3.59	6.25
Dihydroorotate	0.19	0.16	0.14	0.16	0.12	0.07	0.11	0.16	0.11
Erythrose	1.20	0.83	0.64	0.57	0.39	0.14	0.17	0.33	0.35
FAD	0.00	0.00	0.02	0.06	0.11	0.21	0.16	0.22	0.27
Fructose-1,6-bP	21.05	12.67	5.77	2.99	0.78	0.25	0.16	0.16	0.17
Fructose-6-P	46.48	40.82	19.16	10.20	3.92	0.51	0.52	0.37	0.95
Fumarate	2.32	1.78	2.78	1.98	2.37	2.85	3.16	4.32	4.07
GDP	0.38	0.40	0.21	0.19	0.15	0.19	0.15	0.37	0.44
Glucose	39.12	6.55	10.22	1.04	0.34	0.10	0.05	0.04	0.04
Glucose-6-P	23.35	18.96	9.35	5.24	1.95	0.25	0.14	0.28	0.55
Glutamate	500.96	474.08	525.13	321.27	687.17	492.94	433.51	418.71	289.06
Glycerol	15.84	12.55	9.48	5.93	6.55	4.02	3.96	5.52	5.97
Glycine	0.73	1.16	0.91	0.25	6.87	33.45	38.75	3.47	1.36
GMP	0.01	0.08	0.00	0.04	0.04	0.04	0.05	0.29	0.29
GTP	2.01	1.88	1.47	0.96	0.84	0.69	0.74	1.11	1.36
Guanine	0.12	0.07	0.08	0.05	0.06	0.10	0.10	0.16	0.17
Histidine	10.13	2.21	4.71	2.44	7.90	16.16	28.19	124.02	153.18
IMP	0.73	0.62	0.36	0.27	0.12	0.06	0.06	0.07	0.06
Isoleucine	49.70	34.02	41.05	30.92	47.68	24.92	21.19	25.49	20.18
Lactate	17.05	14.70	10.43	13.65	7.66	10.50	8.42	8.55	5.83
Leucine	44.46	29.63	34.79	21.47	25.22	13.39	11.94	13.36	11.58
Lysine	13.54	9.54	10.83	7.71	58.57	152.16	298.38	537.32	741.52
Malate	0.36	0.30	0.23	0.13	0.21	0.23	0.23	0.46	0.61
NAD+	1.05	0.51	0.59	0.42	0.33	0.48	0.34	0.34	0.84
NADP+	2.82	1.66	2.34	1.59	1.24	1.35	0.84	0.95	1.07
Ornithine	0.15	0.10	0.10	0.09	1.04	4.84	11.69	22.25	25.68
Orotate	0.05	0.04	0.04	0.18	0.06	0.02	0.02	0.03	0.02
2-Oxoglutarate	0.78	0.73	1.02	1.05	0.84	0.60	0.43	0.42	0.37
5-Oxoproline	35.51	63.84	41.10	30.73	30.50	17.87	16.03	13.62	11.73
Phenylalanine	19.64	9.84	11.11	5.92	7.26	5.85	6.35	8.10	6.79
Phosphoenolpyruvate	11.05	9.92	9.87	7.12	7.51	12.19	11.23	9.32	7.78
3-Phosphoglycerate	3.46	3.91	5.51	4.97	5.46	13.94	12.79	10.07	6.84
Proline	210.18	158.02	344.37	285.52	585.01	332.55	261.12	282.89	263.20
Pyruvate	3.73	3.95	3.73	2.43	1.51	1.07	0.90	1.33	1.29
Serine	103.24	102.80	123.81	67.40	58.72	26.39	13.42	30.58	21.47
Succinate	2.62	2.31	2.50	1.75	4.63	3.16	2.13	1.50	1.07
Threonine	31.02	26.53	32.18	25.74	52.00	41.50	11.33	0.60	0.35
Thymine	0.20	0.12	0.12	0.11	0.22	0.12	0.14	0.21	0.19
Tryptophan	17.33	5.03	6.77	2.94	5.13	5.42	6.46	13.25	10.71
UDP	0.47	0.70	0.48	0.71	0.64	0.41	0.19	0.45	0.47
UMP	2.88	2.41	1.59	1.52	1.26	0.65	0.63	1.22	1.14
Uracil	0.16	0.09	0.09	0.06	0.12	0.08	0.08	0.12	0.13
Urea	93.10	66.58	34.17	16.73	16.30	13.49	14.63	18.60	11.83
UTP	5.80	5.56	5.35	3.73	2.78	1.38	1.13	1.23	1.24
Valine	65.97	47.26	63.01	51.00	98.47	48.49	50.73	65.03	49.15

starvation. As expected, enzymes of gluconeogenesis increased in level after depletion of glucose (*e.g.* PckA, GapA2), probably indicating strongly increased synthesis. TCC enzymes, such as SdhA and Icd, were also present in higher amounts in the cells during the stationary phase (see Fig. 5 and Table S3, ESI†). In contrast, enzymes of branched-chain amino acid biosynthesis (IlvB, IlvD), purine metabolism (NrdF, PurF) and a ribosomal protein (RplJ) were clearly reduced in concentration in starving cells (Table S3, ESI†). Enzymes of the glycolytic pathway (*e.g.* GapA1, Pgi, Pgk) were present also at reduced levels compared to exponentially growing cells, but their ratios did not fall below the selected threshold (see above). Such reductions in protein amount probably indicate decreased stability because protein levels

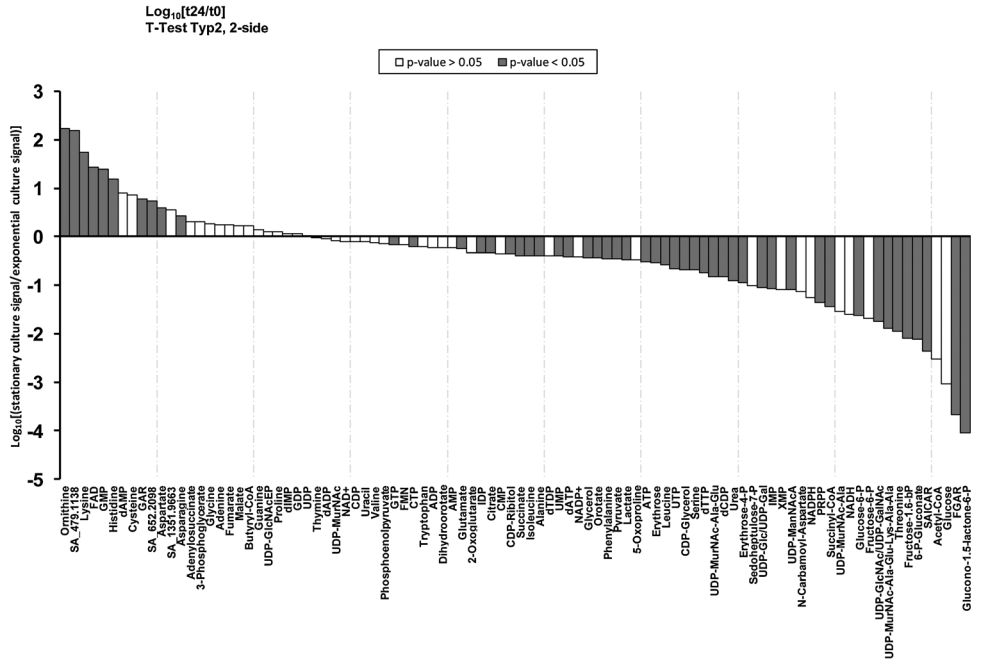

Fig. 3 Alterations in the *S. aureus* metabolome during glucose starvation. The metabolite concentration ratios of cells starved for glucose (stationary culture, t_{24}) and cells growing with glucose (exponential culture, t_0) are plotted. Data represent the average of three independent cultivations. Significant alterations are marked with dark grey (unpaired, two-tailed Student's *t*-test; $p < 0.05$).

should remain constant in non-growing cells even in the absence of new synthesis unless enhanced degradation is observed. One obvious reason for the observed increase in degradation might be the need for the generation of nutrients from proteins no longer needed in non-growing cells. Table S3 (ESI†) summarizes the data for proteins involved in carbon core metabolism and other main metabolic routes. A statistical analysis and graphical visualization of these data using TMEV revealed that out of 92 proteins 21 showed significant time-dependent changes (10 increased and 11 decreased levels, respectively) see Fig. S3 (ESI†) (ANOVA). Fold changes in protein spot intensity ranged from 10-fold decrease (Acs) up to 8.3-fold increase (SucB) when comparing exponentially growing and starving *S. aureus* cells. However, metabolite levels displayed a much wider dynamic range, involving almost complete disappearance (*e.g.* glucono-1,5-lactone-6-P, glucose and FGAR) up to 50- to 170-fold increases in levels (glycine, lysine and ornithine) in the stationary phase compared to exponential growth (Fig. 3). This observation supports the assumption that the metabolome is generally more dynamic than the proteome.

Pathway dependent interpretation of metabolome and proteome profiles

Glycolytic pathways

Under aerobic conditions *S. aureus* catabolizes glucose mainly *via* glycolysis, the Embden–Meyerhof–Parnas (EMP) pathway.[40] There is no evidence for the Entner–Doudoroff (ED) pathway in *S. aureus*. Glucose enters the EMP as glucose-6-phosphate, which is produced intracellularly by glucose kinase activity or mostly by PTS-mediated transport. Fig. 5 gives an overview on the alterations in the concentrations of metabolites involved in EMP, pentose-phosphate pathway (PPP) and neighboring pyruvate pathways, as well as proteins that are associated with these pathways. During growth the intracellular levels of glucose, glucose-6-phosphate, fructose-6-phosphate and fructose-1,6-bisphosphate decreased in parallel to the extracellular glucose consumption. Interestingly, high extracellular concentrations of glucose (mM range) cause high intracellular levels of glycolytic constituents like glucose-6-P ($\sim$20 μmol g^{-1} CDW) and fructose-1,6-bP ($\sim$40 μmol g^{-1} CDW) during exponential growth (OD 0.5), which can be interpreted as indicators of glucose excess. Glycolytic enzymes like Pgi (glucose-6-phosphate isomerase), GapA1 (glyceraldehyde-3-phosphate dehydrogenase) and Pgm (phosphoglycerate mutase) were present in higher amounts during exponential growth, whereas their levels slightly decreased in the stationary phase (see Fig. 5). Entering the stationary phase, enzymes of gluconeogenesis like GapA2 (glyceraldehyde-3-phosphate dehydrogenase), Gpm (phosphoglycerate mutase) and PckA (phosphoenolpyruvate carboxykinase) were present in higher amounts compared to the exponential phase. The strongest increase in level was observed for GapA2, starting in the transient phase (t_7) and continuing during the stationary phase (see also Table S3, ESI†). A link between gluconeogenesis and pyruvate metabolism is demonstrated by Pyc (pyruvate carboxylase) and PckA. These enzymes generate PEP from pyruvate *via* oxalacetate, consuming ATP. Perhaps, both anaplerotic reactions lead to the increase of PEP after glucose is consumed (see Fig. 4B and 5). After exhaustion of glucose, decreased activity of the phosphoenolpyruvate-dependent phosphotransferase system (PTS) might also contribute to PEP accumulation. In parallel, the intracellular concentration of 3-phosphoglycerate increased (3-fold) in the absence of glucose. This is probably pointing to the gluconeogenic

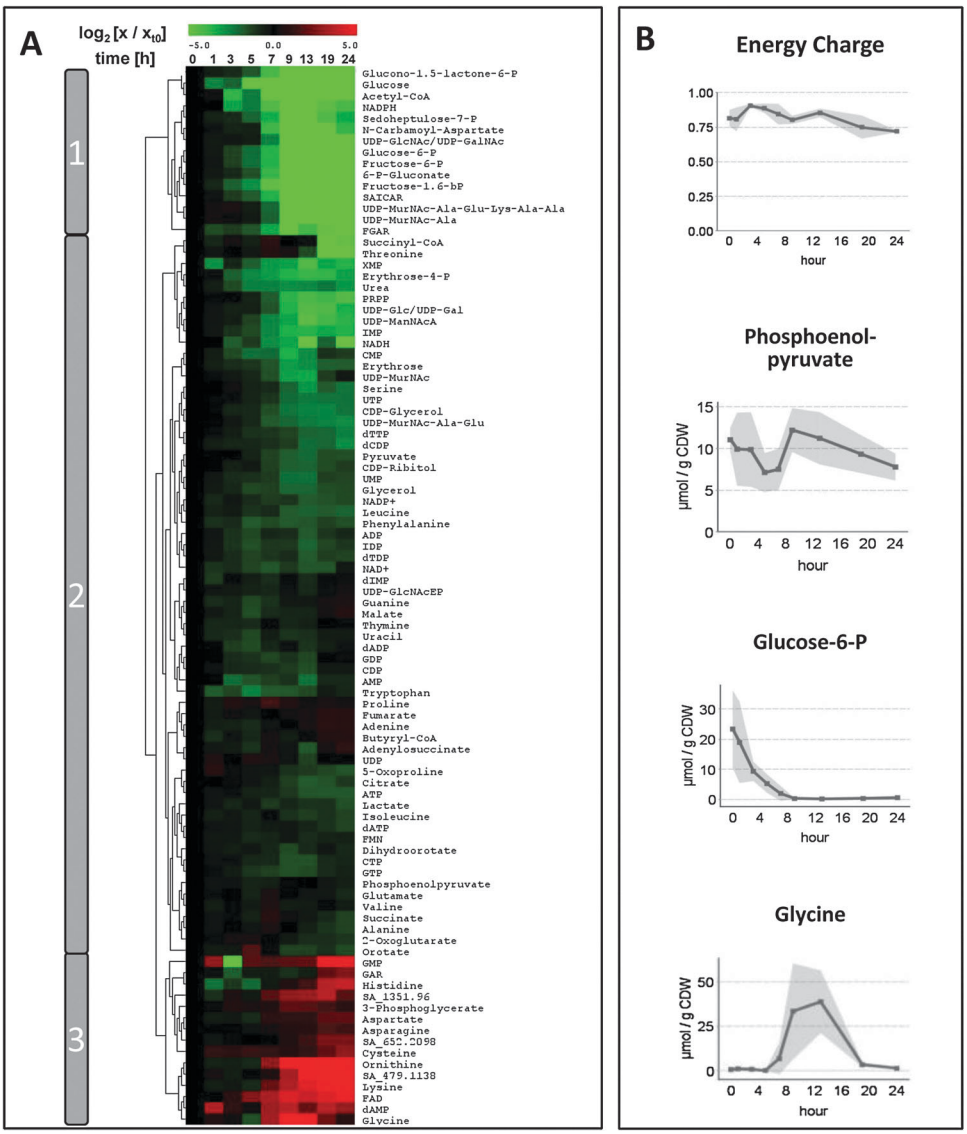

Fig. 4 (A) Presentation of the quantification of all intracellular metabolites identified in *S. aureus* COL grown aerobically in the chemically defined medium. Hierarchical cluster analysis of the metabolite values in course of time was performed with TMEV [$\log_2(x/x_{t0})$]. Changes are displayed by the indicated color coding. Thereby red coloring shows increases in concentrations and green coloring represents decreases in concentrations. The adenylate energy charge (AEC = (1/2[ADP] + [ATP])/([AMP] + [ADP] + [ATP])) and selected metabolites with different kinetics are shown in (B), the grey shadow represents the standard deviation of three biological replicates.

bottleneck, the GapA2 enzyme. It catalyzes the rate limiting step from 1,3-bisphosphoglycerate to glycerinaldehyde-3-P which requires NADPH as well as energy. The intracellular pyruvate level already started to decrease during the transient phase and remained at a low level ($\sim$1 µmol g^{-1} CDW) in the stationary phase (see Table 1). It therefore might be an intracellular marker-metabolite for carbon starvation in *S. aureus* as described for yeast.[41]

Pentose-phosphate pathway

Besides glycolysis, a fueling pathway based on pentoses exists. The reverse pentose-phosphate pathway (PPP) regenerates glyceraldehyde-3-P and fructose-6-P for filling up glycolysis and provides important precursors like erythrose-4-P, sedoheptulose-7-P and pentose-phosphates for nucleic acid and cell wall biosynthesis. During transition from growth to glucose starvation the levels of PPP-enzymes like Zwf (glucose-6-phosphate 1-dehydrogenase) and Tal (transaldolase) as well as Tkt (transketolase) did not significantly change (see Fig. 5 and Table S3, ESI†). On the metabolic level, the intermediates of PPP strongly decreased until glucose was exhausted and no further increase was observed in the stationary phase (Fig. 4).

Pyruvate and overflow metabolism

The central reaction in pyruvate metabolism is catabolized by the pyruvate dehydrogenase multi-enzyme complex, generating acetyl-CoA *via* oxidative decarboxylation. None of the subunits of this complex, *i.e.* PdhA, PdhB, PdhC, PdhD, displayed strong changes in abundance during transition from

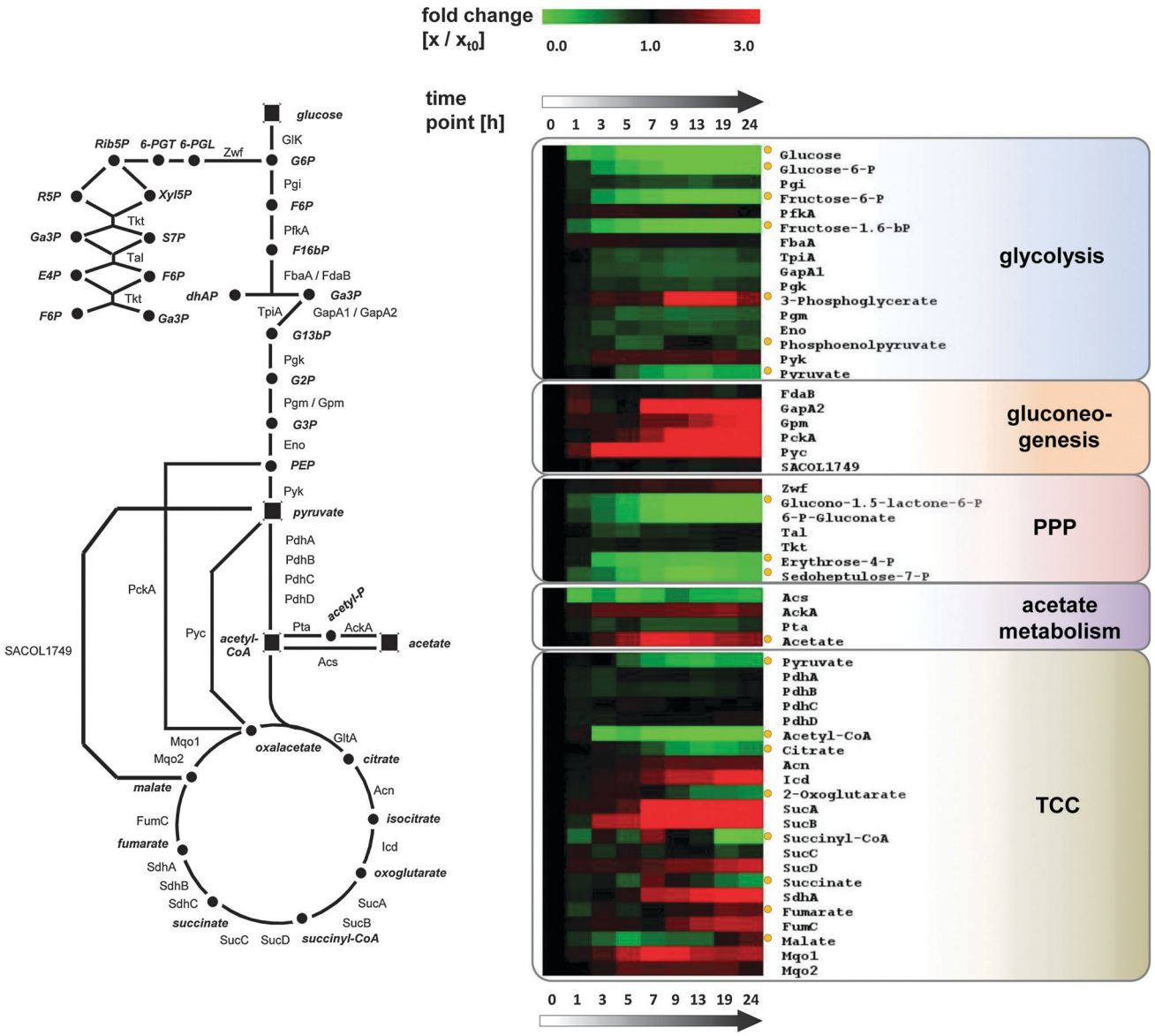

Fig. 5 Combined metabolome and proteome alterations in central carbon pathways during aerobic transition from exponential growth to glucose starvation. Fold changes of respective metabolites and proteins are shown in the order of occurrence in the respective pathway. Metabolites are highlighted with a circle next to the heatmap visualization. For some metabolites/proteins of the pathways, no results could be shown since either they could not be detected by the used techniques or their concentrations were under the limits of detection. The presented fold changes of acetate refer to the analyzed extracellular concentrations.

growth to starvation. However, as previously described pyruvate was secreted under glucose excess.[42] As indicated above intracellular pyruvate levels markedly decreased during starvation in parallel with pyruvate uptake from the medium.

During glucose excess acetyl-CoA was mainly transformed into acetate, most likely by Pta (phosphotransacetylase) and AckA (acetate kinase), and was exported into the medium up to a concentration of $\sim$6 mmol L^{-1} (see Fig. 2A and Table S2a, ESI†). High levels of Pta and AckA were detected during exponential growth. During stationary phase excreted acetate was utilized from the medium. Interestingly, in our experiments the acetyl-CoA-synthetase (Acs) was present at very low levels during exponential growth and further decreased in concentration during starvation. Furthermore the intracellular concentration of acetyl-CoA constantly decreased until the stationary phase. This is most likely caused by the lack of glucose and the subsequent reduction in glycolytic activity. The acetyl-CoA concentrations did not increase in spite of acetate uptake during the stationary growth phase. Compared to organisms with an intact glyoxylate shunt for utilizing C_2-compounds, like *Bacillus licheniformis*, the acetate reconsumption in *S. aureus* is incomplete. In contrast, for *S. aureus* it is assumed that acetate is channeled back into the TCC *via* acetyl-CoA.[43]

Tricarboxylic acid cycle

Compared to the overall metabolite concentrations, intermediates of the TCC were present in low concentrations

during growth at less than 1.0 μmol g^{-1} CDW for malate and up to ~5.0 μmol g^{-1} CDW for citrate and succinate (see Table 1). During starvation all TCC intermediates decreased, except for malate and fumarate. Simultaneously, higher protein amounts were observed for most of the TCC enzymes in the stationary phase by 2D-gel analysis (see. Fig. 5 and Table S3, ESI†). Accumulation was especially strong for the two subunits of the 2-oxoglutarate dehydrogenase (SucA/SucB). Increased accumulation of TCC enzymes is probably caused by relief from repression by CcpA which has been shown to directly control transcription of genes of the TCC enzymes in *S. aureus*.[44] Repression of expression of genes encoding TCC enzymes might be particularly strong in *S. aureus* cultivated in CDM due to the presence of multiple amino acids, which reduces the requirement of TCC for energetic or anabolic functions like amino acid synthesis.[45,46] After exhaustion of glucose, TCC is required to reutilize the secreted overflow metabolites like organic acids and acetate.

Amino acid metabolism

Since *S. aureus* growing in CDM was supplied with a complex mixture of 15 amino acids, uptake is preferred compared to *de novo* synthesis (see Fig. 2). Furthermore, the intracellular pool of amino acids can be replenished by proteolysis in glucose-starved *S. aureus* cells.[47] Fig. 6 offers a general overview of the amino acids profile during exponential growth, in the transition phase or during glucose starvation. In general, it can be stated that externally added amino acids were detected in higher amounts intracellularly. Amino acids not provided in CDM, *e.g.* asparagine and glycine, were only detected in traces during exponential growth; methionine and tyrosine were not detected intracellularly. In growing *S. aureus* cells the intracellular amino acid pool was dominated by glutamate, alanine, proline and aspartate (~500, 300, 200, 150 μmol g^{-1} CDW, respectively) (see Fig. 6). Intermediate concentrations were observed for the branched-chain amino acids leucine, isoleucine, and valine (~50 μmol g^{-1} CDW). The aromatic amino acids histidine, phenylalanine, and tryptophan were present at ~10 μmol g^{-1} CDW. Thus, despite the fact that those amino acids were all present in the growth medium at around 1 mmol L^{-1}, quite different steady state concentrations were reached intracellularly. However, intracellular amino acid pools displayed pronounced alterations during the transition from exponential growth to starvation (see Fig. 6). These alterations were not only strong in terms of fold changes, but also altered the ranking of most prominent intracellular amino acids significantly. Lysine for example increased from ~10 up to ~700 μmol g^{-1} CDW and was therefore the major intracellular amino acid during carbon starvation. Probably, this increase was driven by enhanced uptake because starving *S. aureus* cells have been shown to display a higher uptake of lysine, driven by the proton motive force, in exchange with potassium.[48] Enzymes of lysine biosynthesis such as DapA, DapB, DapD (dihydrodipicolinate synthases), SACOL1801 and LysA (diaminopimelate decarboxylase) showed no significant change in level during the transition from growth to starvation. Histidine as a basic amino acid also exhibited a remarkable accumulation (15-fold) in the stationary phase, probably mediated by uptake because *S. aureus* is not able to synthesize histidine (see Fig. 6). An increased aspartate concentration was also observed, reaching 590 μmol g^{-1} CDW. Glutamate belonged to the highly abundant amino acid group both in growing as well as starving cells reflecting its role as the main connection between nitrogen and carbon metabolism. However, in the stationary phase the glutamate pool slowly declined. Cysteine levels increased in the stationary phase, which coincided with a higher CysK (cysteine synthase) level (see Table S3, ESI†, and Fig. 6). This thiol group containing amino acid is suggested to support an elevated oxidative stress resistance, as recently shown for diamide stressed *Bacillus subtilis* and *S. aureus*.[49] Stationary phase cells of *S. aureus* display an increased tolerance against oxidative stress.[50] Consistent with that we observed slightly elevated levels of oxidative stress protective proteins like AhpC (alkyl hydroperoxide reductase) and KatA (catalase) (Table S3, ESI†).

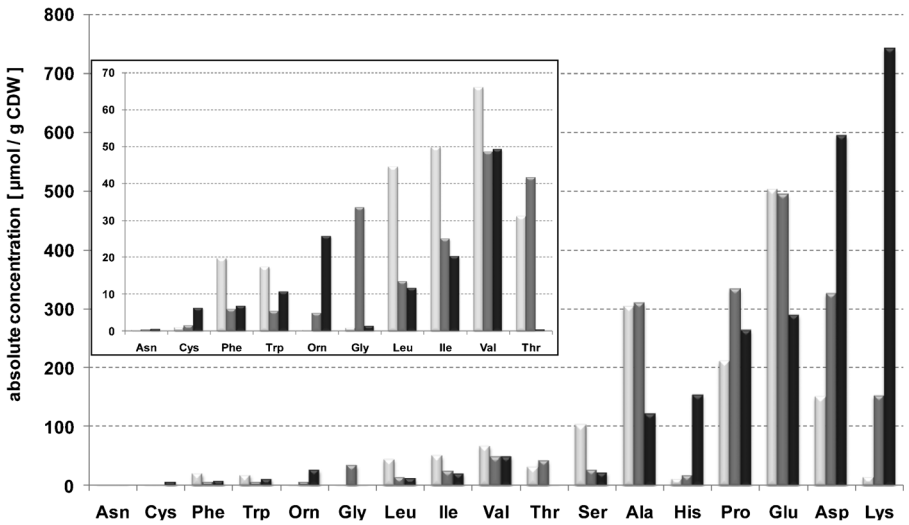

Fig. 6 Intracellular amino acid pools of *S. aureus* during different growth phases. Amino acid concentrations of the exponential growth phase (t_0) are displayed in light grey bars, the transient growth phase (t_9) concentrations are shown in grey bars and the stationary growth phase (t_{24}) concentrations are shown in dark grey bars.

S. aureus has been predicted to be able to use amino acids as alternative carbon sources[10] and an increase in the level of amino acid degrading enzymes and the expression of the encoding genes was observed after glucose depletion.[44] Extracellular serine, threonine and alanine levels already started to significantly decrease during growth, probably by utilization of amino groups in the urea cycle. Urea as a byproduct decreased concomitantly with the glucose concentration (see Fig. S4, ESI†) due to urease activity. The subunit UreC is present in considerable amounts during exponential growth and its level decreased drastically after entry into the stationary phase (see Table S3, ESI†). As recently shown by Michalik *et al.*,[47] urease (especially subunit UreC) undergoes strong proteolysis after glucose depletion. However, extracellular urea levels remained constant and at best slightly increased in the late stationary phase but did not change significantly despite the degradation of UreC (data not shown). After glucose exhaustion, ornithine, another byproduct in this pathway, showed a strong increase.

A particular pattern was observed for the intracellular glycine pool. Only traces could be detected until glucose was completely consumed. This is probably due to high flux rates of glycine into downstream pathways. Transiently, with the exhaustion of glucose and simultaneously with the cessation of growth, the glycine level increased 20-fold for approximately 6 hours, followed by a rather sharp decline to the original low basal level (see Fig. 4B). Probably, this transient increase is related to a stop or decrease in purine/pyrimidine or cell wall biosynthesis after glucose depletion, because in both pathways glycine serves as an important precursor. Another possibility is serine degradation to glycine and 5,10-methylene-tetrahydrofolate, which serves as important C_1 body for many biosyntheses.

Purine/pyrimidine metabolism

Fast growth requires intense synthesis of macromolecules such as DNA and RNA, which in turn depends on the availability of purines and pyrimidines. Syntheses of both purines and pyrimidines are therefore precisely adjusted to environmental conditions.[21,51] In general, adenosine nucleotides were present at higher levels than, for example, guanosine nucleotides (AXPs : GXPs $\approx$ 10 : 1) (Table 1). The level of metabolites related to nucleotide synthesis decreased during transition to and during the stationary phase (see Fig. 4A), like PRPP (Table S2b, ESI†). However, focusing on central fueling pathways and their regulation, the adenosine phosphate ratios play a major role, mathematically expressed by the adenylate energy charge AEC = (1/2[ADP] + [ATP])/([AMP] + [ADP] + [ATP]). Under normal non-limiting conditions a bacterial cell holds its AEC in a narrow range of 0.80 to 0.95.[52] Such values were also determined in our experimental setup as long as *S. aureus* grew, afterwards the AEC dropped slowly but continuously finally reaching an AEC below 0.8 (late stationary phase) (see Fig. 4B). The AEC is probably reduced in starving cells because fueling pathways cannot provide ATP despite the strongly reduced consumption.

Furthermore, pyrimidine nucleotides serve as precursors for *e.g.* cell wall biosynthesis. Cytidine nucleotide (wall teichoic acid synthesis) and uridine nucleotide (peptidoglycan synthesis) levels decreased permanently until the stationary phase.

Cell wall biosynthesis

Most of the precursors that are needed for the synthesis of peptidoglycan and teichoic acids were detected in our study and displayed growth phase-dependent alterations in levels. When the bacterial cells ceased growth less precursors of peptidoglycan biosynthesis, *e.g.* UDP-N-MurNAc-Ala, UDP-MurNAc-Ala-Glu and UDP-MurNAc-pentapeptide were detected, indicating adjustment of levels to the cell's reduced needs (see Fig. 4A and Table S2b, ESI†). The activated precursors for wall teichoic acid biosynthesis, CDP-glycerol or CDP-ribitol, behaved similarly, except UDP-MurNAc. After glucose depletion this compound increased to the initial amount at the exponential phase (Fig. 4A). The turnover reaction to UDP-MurNAc-Ala by MurC (UDP-MurNAc-alanine-ligase) is ATP dependent; probably the decreased energy charge inhibits this pathway. The amount of MurC as well as other enzymes involved in cell wall biosynthesis did not change during the experiment. One exception was MurAA, which catalyzes the first committed step in peptidoglycan biosynthesis, and which decreased in the stationary phase (Table S3, ESI†). In long term starved *S. aureus* COL cells and in *B. subtilis* this enzyme was shown to be the target for proteolysis.[47,53]

Conclusion

This report combines for the first time metabolome and proteome data from a time resolved study to gain insight into the adaption of *S. aureus* towards glucose starvation. In general, changes in the proteome were in agreement with the metabolome, but the metabolic profile displayed a much wider dynamic range. In exponentially growing cells the highly active glycolysis led to a vast accumulation of extracellular acetate, while the TCC was repressed by glucose mediated carbon catabolite repression. Interestingly, intermediates of TCC were secreted into the medium under these repressive conditions, showing a basal TCC activity as an anabolic pathway. Following exhaustion of glucose, levels of TCC and gluconeogenic enzymes increased (Fig. 5). ATP generation by substrate level phosphorylation in the glycolysis was no longer available and was compensated by NADH generation *via* TCC with subsequent ATP production by oxidative phosphorylation. The adenylate energy charge dropped only slightly during the stationary phase (see Fig. 4B). This observation complies with recent data from yeast under different starvation conditions, whereas only in phosphate limited cells the energy charge drops drastically in contrast to carbon or nitrogen starvation.[41]

After extracellular glucose was depleted, *S. aureus* reused secreted overflow metabolites like acetate and pyruvate. In order to do so, in the absence of the glyoxylate cycle a fully functional TCC is needed to catabolize acetate.[43] In agreement with the release of TCC genes from CcpA mediated repression, extracellular TCC intermediates were reused in the stationary phase, probably imported by a specific H^+ symporter, energized by an electrochemical proton potential.[54] Additionally,

the consumption of amino acids was enhanced in glucose starved cells. Different uptake patterns were observed, indicating versatile roles of the supplied amino acids. One strongly consumed group, consisting of alanine, serine and threonine, served as additional carbon sources for *S. aureus*, accompanied by remarkable intracellular threonine exhaustion. Another group of amino acids showed negligible consumption although they were necessary for growth (*e.g.* valine, tryptophan, phenylalanine, proline) and possibly used directly in protein biosynthesis. Most striking was the intracellular accumulation of different amino acids in the stationary phase, *e.g.* lysine, aspartate, histidine and ornithine (see Fig. 6). Since biosynthetic pathways showed no significant alterations on the proteome level, we assume that uptake of lysine and histidine compensated intracellular pH imbalances by proton influx through the ATP-generating proton motive force in glucose depleted cells.[48,55] Due to a stop in nucleotide synthesis, accumulation of aspartate and the glycine alterations may occur. Ornithine increased 170-fold from the early exponential until the stationary phase as a result of amino acid degradation *via* the urea cycle. Overall the amino acid pool showed the most pronounced alterations in terms of intracellular concentrations during glucose starvation. In comparison intermediates of glycolysis, PPP and TCC also showed strong fold changes but their overall amount was significantly lower. The metabolite levels found for *S. aureus* in this study exhibited distribution comparable to those quantified in *E. coli*.[16] Such data are of utmost importance for metabolic network constructions and validations.[15,19,20] Surprisingly some concentrations were not in the range expected, *e.g.* glycolytic intermediates were only present at relatively low levels. However, this finding can probably be resolved if one assumes the existence of protein complexes like the glycosome in *B. subtilis*[56] or yeast.[57,58] Protein complexes will allow effective channeling of substrates even in the presence of very low effective intracellular concentrations.[59]

The transition from an exponential growth to a non-growing state requires complex adjustments of cell physiology including synthesis of cell wall intermediates, membranes and proteins as well as energy generation and pH homeostasis. For *S. aureus*, alterations in amino acid pools and consumption were particularly pronounced probably due to adaptation of *S. aureus* to the host, where peptides and amino acids are probably available at higher levels than glucose. It is obvious that some metabolite concentrations will have a cut-off level for secretion or regulation of pathways and thus act as marker metabolites. These types of metabolite signals/concentrations are certainly critical for the proper adaptation of bacteria to environmental cues in the host, and thus the combined metabolic and proteomic profiling will now have to be extended by studying other physiological stress adaptation settings.

Author contributions

MiLa, DZ, SF, MaLi and KD conceived the study. SF, DZ and KD performed experiments. KD analyzed and interpreted the intracellular metabolome data. MaLi and KD analyzed and interpreted the extracellular metabolome data. DZ analyzed the proteome samples and DZ, SF, JB, JPF, SE, UV and MH interpreted the proteome data. TD, UL, RB, UV and MH provided input for the integrative analysis of the data. MaLi, KD, DZ, UV and MiLa wrote the manuscript with input from all authors.

Abbreviations

TCC	tricarboxylic acid cycle
PPP	pentose-phosphate pathway
NMR	nuclear magnetic resonance
GC	gas chromatography
LC	liquid chromatography
MS	mass spectrometry

Acknowledgements

We thank J. Stülke for reading the manuscript and helpful suggestions. For laboratory help and technical experience we are grateful to Hanna Meyer. This work was supported by grants from the Deutsche Forschungsgemeinschaft (SFB/TRR-34) and the Bundesministerium für Bildung und Forschung (BaCell-SysMO 0313978A and BaCell-SysMO2 0315784A). M. Liebeke was the recipient of a fellowship from the Alfried Krupp von Bohlen and Halbach-Stiftung: "A Functional Genomics Approach in Infection Biology".

The authors declare that they have no conflict of interest.

References

1 F. D. Lowy, *N. Engl. J. Med.*, 1998, **339**, 520–532.
2 R. P. Novick, *Mol. Microbiol.*, 2003, **48**, 1429–1449.
3 A. L. Sonenshein, *Nat. Rev. Microbiol.*, 2007, **5**, 917–927.
4 B. Gorke and J. Stulke, *Nat. Rev. Microbiol.*, 2008, **6**, 613–624.
5 K. Pohl, P. Francois, L. Stenz, F. Schlink, T. Geiger, S. Herbert, C. Goerke, J. Schrenzel and C. Wolz, *J. Bacteriol.*, 2009, **191**, 2953–2963.
6 C. D. Majerczyk, M. R. Sadykov, T. T. Luong, C. Lee, G. A. Somerville and A. L. Sonenshein, *J. Bacteriol.*, 2008, **190**, 2257–2265.
7 Y. Zhu, Y. Q. Xiong, M. R. Sadykov, P. D. Fey, M. G. Lei, C. Y. Lee, A. S. Bayer and G. A. Somerville, *Infect. Immun.*, 2009, **77**, 4256–4264.
8 M. R. Sadykov, T. A. Mattes, T. T. Luong, Y. Zhu, S. R. Day, C. D. Sifri, C. Y. Lee and G. A. Somerville, *J. Bacteriol.*, 2010, **192**, 1459–1462.
9 G. A. Somerville and R. A. Proctor, *Microbiol. Mol. Biol. Rev.*, 2009, **73**, 233–248.
10 M. Kuroda, T. Ohta, I. Uchiyama, T. Baba, H. Yuzawa, I. Kobayashi, L. Cui, A. Oguchi, K. Aoki and Y. Nagai, *et al.*, *Lancet*, 2001, **357**, 1225–1240.
11 B. A. Diep, S. R. Gill, R. F. Chang, T. H. Phan, J. H. Chen, M. G. Davidson, F. Lin, J. Lin, H. A. Carleton and E. F. Mongodin, *et al.*, *Lancet*, 2006, **367**, 731–739.
12 S. R. Gill, D. E. Fouts, G. L. Archer, E. F. Mongodin, R. T. Deboy, J. Ravel, I. T. Paulsen, J. F. Kolonay, L. Brinkac and M. Beanan, *et al.*, *J. Bacteriol.*, 2005, **187**, 2426–2438.
13 D. Becher, K. Hempel, S. Sievers, D. Zuhlke, J. Pane-Farre, A. Otto, S. Fuchs, D. Albrecht, J. Bernhardt and S. Engelmann, *et al.*, *PLoS One*, 2009, **4**, e8176.
14 R. Schwarz, C. Liang, C. Kaleta, M. Kuhnel, E. Hoffmann, S. Kuznetsov, M. Hecker, G. Griffiths, S. Schuster and T. Dandekar, *BMC Bioinformatics*, 2007, **8**, 313.
15 M. Heinemann, A. Kummel, R. Ruinatscha and S. Panke, *Biotechnol. Bioeng.*, 2005, **92**, 850–864.
16 B. D. Bennett, E. H. Kimball, M. Gao, R. Osterhout, S. J. Van Dien and J. D. Rabinowitz, *Nat. Chem. Biol.*, 2009, **5**, 593–599.
17 Y. Ohashi, A. Hirayama, T. Ishikawa, S. Nakamura, K. Shimizu, Y. Ueno, M. Tomita and T. Soga, *Mol. BioSyst.*, 2008, **4**, 135–147.

18 M. J. van der Werf, K. M. Overkamp, B. Muilwijk, M. M. Koek, B. J. C. van der Werff-van der Vat, R. H. Jellema, L. Coulier and T. Hankemeier, *Mol. BioSyst.*, 2008, **4**, 315–327.
19 S. A. Becker and B. O. Palsson, *BMC Microbiol.*, 2005, **5**, 8.
20 D. S. Lee, H. Burd, J. Liu, E. Almaas, O. Wiest, A. L. Barabasi, Z. N. Oltvai and V. Kapatral, *J. Bacteriol.*, 2009, **191**, 4015–4024.
21 C. Kohler, S. Wolff, D. Albrecht, S. Fuchs, D. Becher, K. Buttner, S. Engelmann and M. Hecker, *Int. J. Med. Microbiol.*, 2005, **295**, 547–565.
22 W. M. Shafer and J. J. Iandolo, *Infect. Immun.*, 1979, **25**, 902–911.
23 S. Gertz, S. Engelmann, R. Schmid, K. Ohlsen, J. Hacker and M. Hecker, *Mol. Gen. Genet.*, 1999, **261**, 558–566.
24 S. Fuchs, J. Pane-Farre, C. Kohler, M. Hecker and S. Engelmann, *J. Bacteriol.*, 2007, **189**, 4275–4289.
25 H. Meyer, M. Liebeke and M. Lalk, *Anal. Biochem.*, 2010, **401**, 250–259.
26 M. Liebeke, V. S. Brozel, M. Hecker and M. Lalk, *Appl. Microbiol. Biotechnol.*, 2009, **83**, 161–173.
27 S. Donat, K. Streker, T. Schirmeister, S. Rakette, T. Stehle, M. Liebeke, M. Lalk and K. Ohlsen, *J. Bacteriol.*, 2009, **191**, 4056–4069.
28 M. Liebeke, H. Meyer, S. Donat, K. Ohlsen and M. Lalk, *Chem. Biol.*, 2010, **17**, 820–830.
29 M. Liebeke, D. C. Pöther, N. van Duy, D. Albrecht, D. Becher, F. Hochgrafe, M. Lalk, M. Hecker and H. Antelmann, *Mol. Microbiol.*, 2008, **69**, 1513–1529.
30 B. Bunk, M. Kucklick, R. Jonas, R. Munch, M. Schobert, D. Jahn and K. Hiller, *Bioinformatics*, 2006, **22**, 2962–2965.
31 B. H. Junker, C. Klukas and F. Schreiber, *BMC Bioinformatics*, 2006, **7**, 109.
32 A. I. Saeed, V. Sharov, J. White, J. Li, W. Liang, N. Bhagabati, J. Braisted, M. Klapa, T. Currier and M. Thiagarajan, *et al.*, *BioTechniques*, 2003, **34**, 374–378.
33 B. Starcher, *Anal. Biochem.*, 2001, **292**, 125–129.
34 K. Buttner, J. Bernhardt, C. Scharf, R. Schmid, U. Mader, C. Eymann, H. Antelmann, A. Volker, U. Volker and M. Hecker, *Electrophoresis*, 2001, **22**, 2908–2935.
35 M. Berth, F. M. Moser, M. Kolbe and J. Bernhardt, *Appl. Microbiol. Biotechnol.*, 2007, **76**, 1223–1243.
36 C. Kohler, C. von Eiff, G. Peters, R. A. Proctor, M. Hecker and S. Engelmann, *J. Bacteriol.*, 2003, **185**, 6928–6937.
37 S. Schlag, S. Fuchs, C. Nerz, R. Gaupp, S. Engelmann, M. Liebeke, M. Lalk, M. Hecker and F. Gotz, *J. Bacteriol.*, 2008, **190**, 7847–7858.
38 G. A. Somerville, B. Said-Salim, J. M. Wickman, S. J. Raffel, B. N. Kreiswirth and J. M. Musser, *Infect. Immun.*, 2003, **71**, 4724–4732.
39 L. W. Sumner, A. Amberg, D. Barrett, M. H. Beale, R. Beger, C. A. Daykin, T. W. M. Fan, O. Fiehn, R. Goodacre and J. L. Griffin, *et al.*, *Metabolomics*, 2007, **3**, 211–221.
40 H. J. Blumenthal, C. F. Huettner and F. A. Montiel, *Ann. N. Y. Acad. Sci.*, 1974, **236**, 105–114.
41 V. M. Boer, C. A. Crutchfield, P. H. Bradley, D. Botstein and J. D. Rabinowitz, *Mol. Biol. Cell*, 2009, **21**, 198–211.
42 T. S. Theodore and A. L. Schade, *J. Gen. Microbiol.*, 1965, **40**, 385–395.
43 G. A. Somerville, M. S. Chaussee, C. I. Morgan, J. R. Fitzgerald, D. W. Dorward, L. J. Reitzer and J. M. Musser, *Infect. Immun.*, 2002, **70**, 6373–6382.
44 K. Seidl, S. Muller, P. Francois, C. Kriebitzsch, J. Schrenzel, S. Engelmann, M. Bischoff and B. Berger-Bachi, *BMC Microbiol.*, 2009, **9**, 95.
45 H. Ludwig, G. Homuth, M. Schmalisch, F. M. Dyka, M. Hecker and J. Stulke, *Mol. Microbiol.*, 2001, **41**, 409–422.
46 M. S. Rosenkrantz, D. W. Dingman and A. L. Sonenshein, *J. Bacteriol.*, 1985, **164**, 155–164.
47 S. Michalik, M. Liebeke, D. Zuhlke, M. Lalk, J. Bernhardt, U. Gerth and M. Hecker, *Proteomics*, 2009, **9**, 4468–4477.
48 D. F. Niven, R. E. Jeacocke and W. A. Hamilton, *FEBS Lett.*, 1973, **29**, 248–252.
49 D. C. Pöther, M. Liebeke, F. Hochgrafe, H. Antelmann, D. Becher, M. Lalk, U. Lindequist, I. Borovok, G. Cohen and Y. Aharonowitz, *et al.*, *J. Bacteriol.*, 2009, **191**, 7520–7530.
50 S. P. Watson, M. O. Clements and S. J. Foster, *J. Bacteriol.*, 1998, **180**, 1750–1758.
51 B. Fleury, W. L. Kelley, D. Lew, F. Gotz, R. A. Proctor and P. Vaudaux, *BMC Microbiol.*, 2009, **9**, 76.
52 A. G. Chapman, L. Fall and D. E. Atkinson, *J. Bacteriol.*, 1971, **108**, 1072–1086.
53 H. Kock, U. Gerth and M. Hecker, *Mol. Microbiol.*, 2004, **51**, 1087–1102.
54 Z. Tynecka, I. Korona-Glowniak and R. Los, *Arch. Microbiol.*, 2001, **176**, 143–150.
55 T. G. Patton, S. J. Yang and K. W. Bayles, *Mol. Microbiol.*, 2006, **59**, 1395–1404.
56 F. M. Commichau, F. M. Rothe, C. Herzberg, E. Wagner, D. Hellwig, M. Lehnik-Habrink, E. Hammer, U. Volker and J. Stulke, *Mol. Cell. Proteomics*, 2009, **8**, 1350–1360.
57 K. van Eunen, J. Bouwman, A. Lindenbergh, H. V. Westerhoff and B. M. Bakker, *FEBS J.*, 2009, **276**, 5521–5536.
58 F. J. Bruggeman, J. de Haan, H. Hardin, J. Bouwman, S. Rossell, K. van Eunen, B. M. Bakker and H. V. Westerhoff, *Syst. Biol.*, 2006, **153**, 318–322.
59 F. M. Meyer, J. Gerwig, E. Hammer, C. Herzberg, F. M. Commichau, U. Volker and J. Stulke, *Metab. Eng.*, 2011, **13**, 18–27.